# Method of Calculating Band Shape for Molecular Electronic Spectra

**GREG M. PEARL,[1] M. C. ZERNER,[1] ANDERS BROO,[2] JOHN McKELVEY[3]**

[1] *Quantum Theory Project, University of Florida, Gainesville, Florida 32611-8435*
[2] *Department of Physical Chemistry, Chalmers University of Technology, Göteborg, Sweden*
[3] *Image Research and Advanced Development, Eastman Kodak Company, Rochester, New York*

*Received 15 July 1997; accepted 30 December 1997*

**ABSTRACT:** A method for approximating the band shape of molecular electronic transitions based on a single geometric configuration is described. The band shape is modeled using an empirical parameter to estimate the width at half-height for each transition. In addition to generating a shape for allowed transitions, a procedure is developed for approximating the oscillator strength for the symmetry forbidden bands. The results obtained using these two approximations are then compared with experimental spectra and to the results obtained from stochastic methods for simple organic molecules, such as benzene, naphthalene, and the diazobenzenes. © 1998 John Wiley & Sons, Inc. J Comput Chem 19: 781–796, 1998

**Keywords:** molecular electronic spectroscopy; band shape; solvent effects; stochastic methods, ZINDO

## Introduction

Absorption spectroscopy has become a widely utilized tool for chemical analysis and characterization of molecules. Although there are several different types of absorption spectroscopy, we are primarily interested here in UV/visible spectroscopy, which is generated through electronic excitations.

Observed spectroscopic peaks are characterized by their transition frequency ($\nu$), intensities or oscillator strength ($f_{osc}$), and band shape. Although each of these properties can provide valuable information for characterization of a molecule, it has been generally accepted that the frequency is the most important property for chemical analysis. For this reason, theory has been aimed principally at calculating the transition energy, and several successful methods have been developed.[1–6] Al-

*Correspondence to*: M. C. Zerner
Contract/grant sponsor: Eastman Kodak Co.
Contract/grant sponsor: Office of Naval Research
Contract/grant sponsor: IBM; contract/grant number: SUR-96


© 1998 John Wiley & Sons, Inc.
CCC 0192-8651 / 98 / 070781-16

though transition strength and shape have not been considered as vital for chemical analysis, they have certainly not been completely neglected.[1–3a,7–14] Very early it was recognized that the intensity of a transition can be as important in assigning spectra as transition energy, and this is especially so when close-lying bands are calculated in the reverse order, but transition strength and its polarization can provide definitive proof. The methods available for predicting band shapes are often restricted to small systems as they generally involve statistical mechanics,[11–14] or use an accurate treatment of the potential and attempt to solve the nuclear problem on this potential.[7–9]

The focus of this work is to predict the band shape for molecular electronic absorption spectroscopy for large systems in condensed phases.[10a] Under such conditions there are many phenomena that broaden transitions. Perhaps the major contributors for such broadening are the unresolved transitions to the various vibrational levels of the excited state. Vibrational broadening is not the only culprit, however, because there are also excitations to the various rotational levels and anisotropic interactions with the medium (solvent) that are also responsible for line broadening. The excitations to the various rotational levels are also dependent upon temperature, whereas the anisotropic interactions with the solvent are primarily dependent upon the solute and solvent. Besides line broadening there are also several factors that will affect the appearance of the band shape.[10a] These factors include overlapping electronic transitions, along with various perturbations between the excited states such as vibronic and spin–orbit coupling. The effects on the appearance of the spectrum that arises from overlapping transitions are plotted in Figure 2.

In this work we develop an empirical method for reproducing the band shape from a single geometric structure. The procedure described in the theory section of this article is composed of two simple models. The first model approximates the width at half-height for either a Gaussian or Lorenzian band shape, whereas, the the second model allows us to estimate the oscillator strength for symmetry-forbidden transitions. The Gaussian and Lorenzian band shapes are chosen because it is easily shown that low resolution spectroscopic bands possessing unresolved excitations might follow these shapes.[10a]

## Theory

The oscillator strength, a dimensionless quantity, for the $I$th transition is given by[10,14]:

$$f_{osc}(I) = 2/3|\langle\psi_0|\,\mu|\psi_I\rangle|^2\,\Delta E_{0I} \qquad \text{[atomic units]} \tag{1a}$$

$$= 4.709 \times 10^{-7}|\langle\psi_0|\,\mu|\psi_I\rangle|^2\,\Delta E_{0I} \qquad [\text{Debye, cm}^{-1}] \tag{1b}$$

where $\mu$ is the dipole moment operator and $\Delta E$ is the transition energy for the given transition. For comparison, the experimental oscillator strength is calculated by integrating the area under the corresponding $I$th absorption peak:

$$f_{osc}(I) = 4.319 \times 10^{-9} \int \varepsilon(\nu)\,d\nu \tag{2}$$

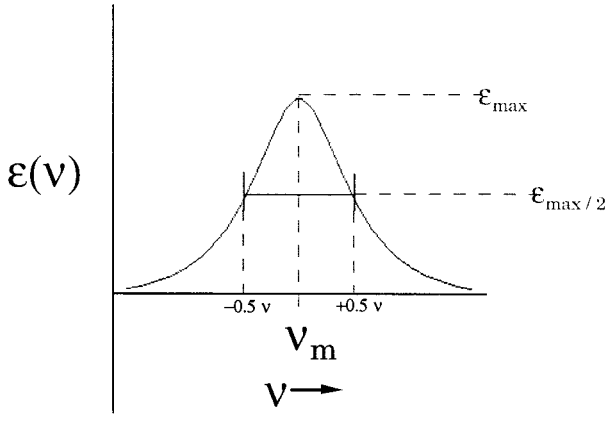


**FIGURE 1.** Anatomy of an ideal spectral peak.

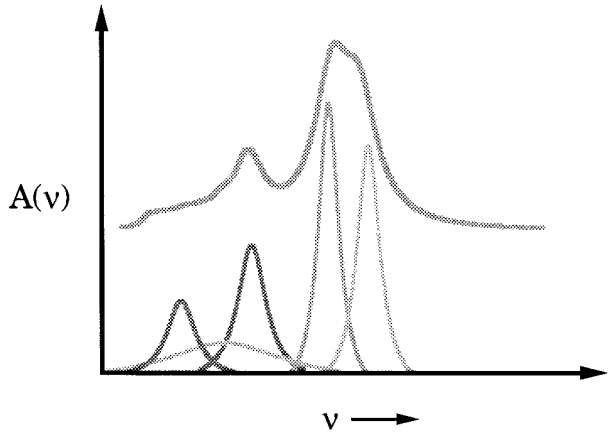


**FIGURE 2.** Band overlapping.

where the molar extinction coefficient $\varepsilon(\nu)$ is given (in units of L mol$^{-1}$ cm$^{-1}$), and also the wave number frequency (cm$^{-1}$).

We have chosen to use the Gaussian functional form for the remainder of this development, although assuming a Lorenzian follows a parallel development. The functional form for the Gaussian is:

$$\varepsilon(\nu) = \bar{\varepsilon}_{max} e^{-\alpha(\nu - \nu_{max})^2} \tag{3}$$

where:

$$\bar{\varepsilon}_{max} = (\epsilon_{max})(4.319 \times 10^{-9}) \tag{4}$$

and $\alpha(I)$ is:

$$\alpha(I) = \frac{\pi \bar{\varepsilon}^2_{max}(I)}{f_{osc}(I)} \tag{5}$$

The calculated oscillator strength is then given by:

$$f_{osc} = \int \bar{\varepsilon}_{max} e^{-\alpha(\nu - \nu_{max})^2} \, d\nu \tag{6}$$

The problem now is to determine a width or a height such that the integrated area yields the calculated oscillator strength when fitted to the Gaussian form.

The width at half-height for a Gaussian, eq. (3), is:

$$\nu_{\pm 1/2} = \nu_{max} \pm \frac{0.836}{\alpha^{1/2}} \tag{7a}$$

or:

$$= \nu_{max} \pm w/2 \tag{7b}$$

These equations are then rearranged to solve for the width ($w$) for each corresponding transition between the ground state (0) and excited state ($I$):

$$w(I) = \frac{1.6651 f_{osc}(I)}{\sqrt{\pi}\, \bar{\varepsilon}_{max}(I)} \tag{8}$$

The spectral width for a given vibrational mode between two atoms (A, B) is then estimated to be:

$$w_{AB}(I) = \langle \Delta q^2_{AB} \rangle^{1/2} \left[ \frac{\partial E(I)}{\partial q_{AB}} \right] \tag{9}$$

In eq. (9), $\langle \Delta q^2_{AB} \rangle^{1/2}$ measures the motion on the ground state potential energy surface by this atom pair, whereas the second term measures the change in energy of the excited state surface with respect to the change in bond distance. Assuming harmonic motion on the ground state potential energy surface, the expectation value of $\Delta q^2_{AB}$ can be derived as:

$$\langle q^2_{AB} \rangle = 2\sqrt{2}\,\hbar [\, K_{AB}\, \mu_{AB}]^{-1/2} \tag{10}$$

where $\mu_{AB}$ is the reduced mass and $K_{AB}$ (cm$^{-1}$/Å$^2$) is the force constant. In general, force constants can be obtained from experiment, or calculated by diagonalizing the calculated mass-weighted Hessian matrix. However, for this work, we have chosen to estimate the force constants from the AMBER force field (Table I).[15] The force constant for a single bond ($K^0_{AB}$) is used as an atom pair parameter, which is scaled according to the square root of the bond order of the appropriate atom pair:

$$K_{AB} = \sqrt{B_{AB}}\, K^0_{AB} \tag{11}$$

The use of such a scaling seems to roughly approximate the relation between single-, double-, and triple-bond $K_{AB}$. The bond index is defined as:

$$B_{AB} = \sum_{\mu}^{A} \sum_{\nu}^{B} P_{\mu\nu} P_{\nu\mu} \tag{12}$$

from the first-order density matrix (**P**) formed from the symmetrical orthogonalized basis:

$$\mathbf{P}_{\mu\nu} = \sum_a C_{\mu a} C_{\nu a} n_a \tag{13}$$

where $n_a$ is the occupation of orbital $\varphi_i$; that is, $n_a = 0$, 1, or 2 and $\varphi_i$ is calculated from the molecular orbital coefficients, $C_{\mu a}$:

$$\varphi_a = \sum \chi_\mu C_{\mu a} \tag{14}$$

**TABLE I.**
**Force Constants.**[a]

| Atom pair | Force constant (kcal / mol · Å$^2$) | Atom pair | Force constant (kcal / mol · Å$^2$) |
|---|---|---|---|
| H—H | 200.0 | C—C | 300.0 |
| H—C | 340.0 | C—N | 280.0 |
| H—N | 434.0 | C—O | 310.0 |
| H—O | 553.0 | C—S | 222.0 |
| H—S | 274.0 | N—O | 300.0 |
| H—S | 274.0 | N—S | 300.0 |
| S—S | 166.0 | S—Ca | 100.0 |
| S—Sr | 300.0 | S—Ce | 200.0 |

[a] From ref. 15 and experimental vibrational frequencies.

This definition of bond order ($B_{AB}$) has the advantage of having the traditional values of 3 for $N_2$, 2 for $O_2$, 1 for $F_2$, etc. The use of eq. (11) permits the use of a single empirical parameter for each pair of atoms and also has the advantage of automatically generating a zero value when there is no bond between the two atoms A and B.

In a more exact treatment of this problem one could evaluate and diagonalize the mass-weighted Hessian matrix, as previously mentioned, to calculate the force constants directly for each normal mode.[16] We have chosen to pursue the approximate method for determining the force constants because we will be interested in very large molecules, and, in addition, the semiempirical model Hamiltonians used to calculate the spectra of larger systems generally overestimate harmonic frequencies. Note, additionally, that we will sum overall atom pairs, rather than normal modes, and this will again introduce some error, as discussed in what follows:

The derivative in eq. (9) is only needed for the displacements specified by the ground state normal modes. This derivative could be calculated for the excited-state CI wave function and then transformed to the ground state normal modes, but this is far from a trivial matter.[17] In the spirit of our approximations of the ground state, we have chosen to approximate this according to:

$$\frac{\partial E(I)}{\partial q_{AB}} \approx \{q_{AB}(0) - q_{AB}(I)\} \times \left\{K^0_{AB}\sqrt{B_{AB}(I)}\right\} \tag{15a}$$

and:

$$\approx Z' \times \{B_{AB}(I) - B_{AB}(0)\}^2 \times \left\{K^0_{AB}\sqrt{B_{AB}(I)}\right\} \tag{15b}$$

where, in eq. (15b), $Z'$ is an empirical parameter that might be dependent upon temperature and solvent. Eq. (15a) is exact, assuming a quadratic potential between A and B. The motivation for using eq. (15b) is as follows:

1. The forces applicable on the excited-state potential surface should be proportional to the change in bond strength between the ground and excited state. The change, if the potential were harmonic, would not depend on the sign of the change. To accomplish this, we take the square of the difference, although it would also be valid to take the difference to any even power or the absolute value of the difference.
2. The derivative on the excited-state surface might then be proportional to $K_{AB}\sqrt{B_{AB}(I)}$, as was the case for the ground state. Figure 3 schematically demonstrates why proportionality to the excited-state bond order, a natural part of this model, is reasonable.

Eq. (9) for each atom pair A–B is then:

$$w_{AB}(I) = Z'(2\sqrt{2}\,\hbar)^{1/2} \frac{K^0_{AB}\sqrt{B_{AB}(I)}}{\left(K^0_{AB}\sqrt{B_{AB}(0)}\,\mu_{AB}\right)^{1/4}} \times [B_{AB}(I) - B_{AB}(0)]^2 \tag{16}$$

The total width for a given transition is then approximated by:

$$w(I) = \sum_{A<B} w_{AB}(I) \tag{17}$$

Strictly speaking, the sum for $w(I)$ should be over the $3n - 6(5)$ normal modes rather than the $n(n-1)/2$ atom pairs. We expect the errors associated with this to be small; the bond stretching (A–B) contributions are the major contributions and are described by the neighboring atom pair interactions, the contributions from bond angles (A–B–C) are accounted for by the A–C pair interactions, and the torsional or dihedral angles (A–B–C–D) interactions are accounted for by the bond stretching terms that are separated by two or more atoms. The remaining extra terms in the $n(n-1)/2$ atom pairs are very small considering the bond orders associated with these extra terms are very small.

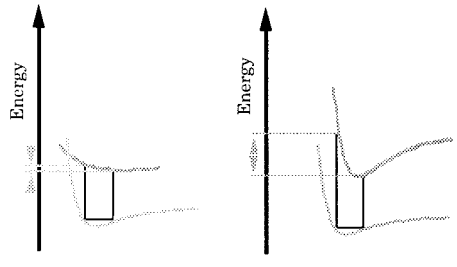


**FIGURE 3.** Effects of the excited state surface on bandwidth.

Using the width from eq. (17) and the calculated oscillator strength from eq. (1), the extinction coefficient and $\alpha$ value are calculated using eqs. (6) and (8). The spectrum is then given by:

$$A(\nu) = \sum_I \bar{\varepsilon}_{max}(I) e^{-\alpha(I)[\nu - \nu_{max}(I)]^2} \tag{18}$$

We also account for dipole forbidden transitions that affect the appearance of the spectrum. These are especially important if the excitations are low lying and not hidden under the allowed bands. These transitions can often borrow intensity from near lying allowed transitions through vibronic coupling. This coupling is approximated by[10a]:

$$|\bar{\psi}_F\rangle = |\psi_F\rangle + \sum_{I \neq F} |\psi_I\rangle C_I \tag{19}$$

$$C_I = \sum_q \frac{\langle \psi_I | \frac{\partial H}{\partial q} | \psi_F \rangle}{(E_F - E_I)} \tag{20}$$

and:

$$\langle \psi_0 | \vec{\mu} | \bar{\psi}_F \rangle = \sum_{I \neq F} \langle \psi_0 | \vec{\mu} | \psi_I \rangle C_I \tag{21}$$

where $|\bar{\psi}_F\rangle$ is the electronically forbidden state of interest and $\langle \psi_0 | \vec{\mu} | \psi_F \rangle = 0$. $|\psi_F\rangle$ can borrow intensity from an allowed state $|\psi_I\rangle$. Eq. (20) results from first-order perturbation theory. The oscillator strength for $|\bar{\psi}_F\rangle$ is now:

$$\bar{f}_F = \tfrac{2}{3} \left| \langle \psi_0 | \vec{\mu} | \bar{\psi}_F \rangle \right|^2 \Delta E_{0F} \tag{22a}$$

$$= \tfrac{2}{3} \left| \sum_{I \neq F} C_I \langle \psi_0 | \vec{\mu} | \psi_I \rangle \right|^2 \Delta E_{0F} \approx \sum_I \bar{f}_F(I) \tag{22b}$$

$$\bar{f}_F(I) = \frac{C_I^2 f_I \Delta E_{0E}}{\Delta E_{0I}} \tag{22c}$$

where we have assumed one state, usually the nearest lying allowed state, dominates in the donation of oscillator strength and we can thus drop the cross terms, as suggested in eq. (22b). We have further assumed that nothing is lost by continuing the sum over all possible states $|\psi_I\rangle$. This approximation relieves us from having to know *a priori* which state is lending the most intensity. A possible side effect of this approximation is that if two or more states contribute sizably to the borrowing, there could be interference (canceling cross terms). This is not likely to be a problem because the transitions that are the most apparent through this mechanism lie at lower transition energies than any of the allowed transitions, and can therefore only borrow from those allowed transitions at higher energies.

The value for $C_I$ is estimated from the geometric mean:

$$C_I = \sum_q \frac{\langle \psi_I | \frac{\partial H}{\partial q} | \psi_F \rangle}{E_F - E_I} \tag{23a}$$

$$\approx Y \sum_q \frac{\langle \psi_I | \frac{\partial H}{\partial q} | \psi_I \rangle^{1/2} \langle \psi_F | \frac{\partial H}{\partial q} | \psi_F \rangle^{1/2}}{E_F - E_I} \tag{23b}$$

$$\approx Y \sum_q \frac{(\partial E(I)/\partial q)^{1/2} (\partial E(F)/\partial q)^{1/2}}{E_F - E_I} \tag{23c}$$

$$\approx Y' \sum_{A<B} K_{AB}^0 \frac{\left( [B_{AB}(I) - B_{AB}(0)]^2 [B_{AB}(F) - B_{AB}(0)]^2 \right)^{1/2} [B_{AB}(I) B_{AB}(F)]^{1/4}}{E_F - E_I} \tag{23d}$$

where $Y' = YZ'^2$ is a second empirical constant. Note that rather cavalier approximations have been made in passing from eq. (23a) to (23b) and then to (23c). These approximations could be totally unfounded in small molecules of high symmetry. In eq. (22b) we use:

$$\bar{f}_F = \sum_{I \neq F} \bar{f}_F(I) \tag{24}$$

If $\tilde{f}_F(I) > 0.1 f_I$, it is then set to $0.1 f_I$. This situation has not occurred in practice, but would occur when first-order perturbation theory is no longer valid, and hence, this entire development would break down.

## Method

The model outlined in the previous section was compared with experiment and with the results of molecular dynamics simulations. The experimental spectra were obtained from the *UV Atlas of Organic Compounds*.[18] The specifics describing the equations of motion for the molecular dynamics, and the Hamiltonian used in the calculation of the energy used in the dynamics, are developed in detail in ref. 19.

The dynamics simulations were performed within the confines of the canonical ensemble (NVT). The target temperature for the dynamics was 300.0 K, with a heat bath friction constant of $\tau = 0.7 \times 10^{-12}$, and a step size of $0.5 \times 10^{-15}$ ps. The dynamics calculations were equilibrated until the $E_{RMS}$ was $< 0.1$ kJ/mol, at which point the calculations were continued for another 50–100 ps. The coordinates used in the last 50–100 ps were outputted to a file every 0.1 ps, and these structures were subsequently used for the quantum-mechanical spectroscopic calculations.

The spectroscopic calculations were all performed with the ZINDO program package[20] using the INDO/S Hamiltonian[6] and the Mataga–Nishimoto empirical two-electron integrals[21] at the CIS level of theory. The number of active orbitals included in the CIS calculations depended upon the specific system being studied, although it was always large enough to include all the active $\pi$ orbitals. In some of the spectroscopic calculations, solvent effects were incorporated into the calculation using a self-consistent reaction field (SCRF).[22] These SCRF calculations were performed using a single spherical cavity with a radius determined from the molar mass of the solute. The SCRF interactions were calculated using the dipole and quadrapole terms.

The calculations from the molecular dynamics were plotted as a histogram of transitions, each fitted to a Lorenzian with a width at half-height of 150 $cm^{-1}$. The empirical bandwidth calculations used a single geometry-optimized structure and the width at half-height specified by eq. (17). The following values were chosen for the empirical band width calculations: $Z' = 67.15$ Å$^2$ [eq. (15b)] and $Y' = 15.00$ Å$^2$ [eq. (23d)].

The ''empirical bandwidth calculation'' using eqs. (18) and (24) required between 8 and 300 CPU seconds on an IBM RS6000, whereas the molecular dynamics simulations followed by the CIS calculation required 15–36 CPU hours on the same machine. The approximate model for obtaining the shape of the spectroscopic peak is thus approximately 1000–10,000 times faster than the current method of using molecular dynamics to obtain band shapes, for these simple systems.

## Results

### BENZENE AND NAPHTHALENE IN NONPOLAR SOLVENTS

The experimental UV/visible spectrum of benzene has two symmetry-forbidden bands, of $^1B_{2u}$ and $^1B_{1u}$ symmetry. These bands are easily observed experimentally, as they are in the molecular dynamics from stochastic sampling over non-$D_{6h}$ structures. Figure 4 shows the experimental spectra along with the plots obtained using molecular dynamics, approximate bandwidth calculation, and the approximate bandwidth calculation without estimating the oscillator strength of the forbidden bands.

The spectra obtained using the molecular dynamics is in very good agreement with experiment as seen in Figure 4. The empirical calculation for benzene should be viewed with some ''skepticism,'' because this was the test molecule that we used for determining the values for the two empirical parameters ($Z'$ and $Y'$). Despite this caveat, the agreement between the empirical calculation, which includes both estimated bandwidth and oscillator strength borrowing, and experiment or molecular dynamics is very good. The numerical values used for creating the spectrum in Figure 4 are listed in Table II. The experimental and calculated spectra for naphthalene are given in Figure 5. Again, as in benzene, the symmetry-forbidden bands have an important role in determining the appearance of the spectrum. A comparison of the two oscillator strengths is presented in Table III.

### COMPARISON OF DIFFERENT SOLVENT FOR PYRIDINE, PYRIMIDINE, AND PYRIDAZINE

The previous sections showed that the empirical bandwidth calculations are capable of modeling

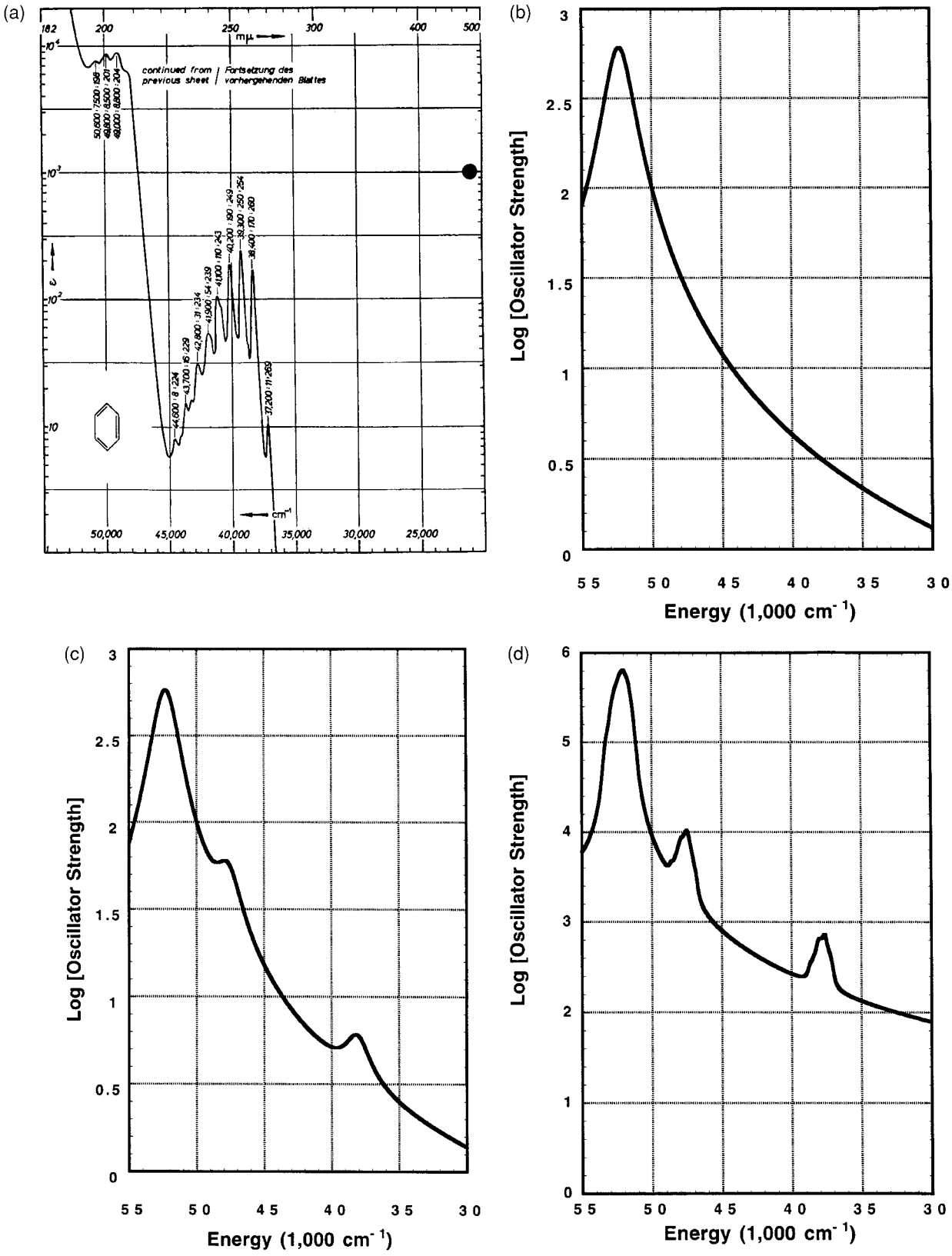


**FIGURE 4.** Benzene spectra. (A) Experimental spectra. (B) Bandwidth results. (C) Bandwidth including estimated vibronic borrowing results. (D) Molecular dynamics results.

**TABLE II.**
**Calculated Benzene Transitions.**

| States | Energy (1000 $cm^{-1}$) | Experiment (1000 $cm^{-1}$) | Width (1000 $cm^{-1}$) | Osc. str. calculated[a] | Osc. str. estimated[a] |
|---|---|---|---|---|---|
| $^1B_{2u}$ | 38.1 | ~ 40 | 2.0 | 0.00 | 0.01 |
| $^1B_{1u}$ | 47.7 | ~ 50 | 2.0 | 0.00 | 0.10 |
| $^1E_u$ | 52.3 ($\times 2$) | ~ 54 | 2.1 | 0.99 | 0.94 |

[a] The calculated oscillator strengths are direct from the quantum mechanics, eq. (1). The estimated oscillator strengths use the calculated oscillator strengths and the approximation of eq. 23.

the appearance of simple organic molecules in nonpolar solvents. We decided to determine if the single empirical parameter $Z'$ is able reproduce several different solvents, or if each solvent requires a significantly different constant. We have chosen to study pyridine, pyrimidine, and pyridazine to test the solvent dependence of $Z'$. These molecules were chosen because they have a permanent dipole and the appearance of the spectrum is known to be somewhat sensitive to different solvents. The nonpolar solvent is modeled with a cyclohexane reaction field. The polar solvent is modeled with a water reaction field, whereas the polar $+n(H_2O)$ is modeled with a reaction field and $n$ water molecules at hydrogen bond distances determined by the quantum chemistry.

The experimental spectrum of pyridine shows that the first observed peak is narrower in water when compared with cyclohexane. This is a consequence of the $n-\pi^*$ excitation being blue shifted under the first allowed $\pi-\pi^*$ transition. This phenomenon is reproduced in the empirical bandwidth calculation. There is a good agreement between the appearance of the experimental and calculated spectra (see Fig. 6). The calculated spectra have also reproduced the deeper minimum between the first and second peak as observed in the experimental spectra.

In Table IV, the calculated peaks along with their corresponding widths at half-height are presented for several different environments. The gas phase entry includes the results obtained without using a reaction field or specific modeling of the solvent. The nonpolar column is obtained from a reaction field modeling cyclohexane for the solvent $\varepsilon = 2.023$, $\eta = 1.4266$. The polar solvent is also a reaction field modeling water for the solvent $\varepsilon = 78.50$, $\eta = 1.3332$. Finally, the polar + $H_2O$ uses the water SCRF and adds either one or two explicit water molecules. These water molecules are placed in hydrogen bonding positions with respect to the solute as determined by the simulation.[22c]

The pyrimidine spectra are also well reproduced, as seen in Figure 7. The first peak, as in pyridine, is narrower in the water spectra when compared with the nonpolar solvent. This trend is again duplicated by the empirical band width calculations, which can be observed in Figure 7 and Table V. Note the rather large differences in calculated widths between polar calculations and the

**TABLE III.**
**Calculated Naphthalene Transitions.**

| States | Energy (1000 $cm^{-1}$) | Experiment (1000 $cm^{-1}$) | Width (1000 $cm^{-1}$) | Osc. str. calculated[a] | Osc. str. estimated[a] |
|---|---|---|---|---|---|
| $^1B_{3u}$ | 32.0 | ~ 32 | 1.4 | 0.004 | 0.004 |
| $^1B_{2u}$ | 35.1 | ~ 35–38 | 3.0 | 0.18 | 0.17 |
| $^1B_{3u}$ | 43.2 | | 1.3 | 1.74 | 1.31 |
| $^1B_{1g}$ | 44.2 | | 3.5 | 0.00 | 0.24 |
| $^1A_g$ | 44.5 | ~ 45 | 1.5 | 0.00 | 0.23 |
| $^1B_{2u}$ | 46.1 | | 1.6 | 0.63 | 0.49 |
| $^1B_{2g}$ | 49.0 | | 2.0 | 0.00 | 0.04 |
| $^1B_{1g}$ | 49.9 | | 3.5 | 0.00 | 0.06 |
| $^1A_g$ | 53.7 | | 2.7 | 0.00 | 0.02 |

[a] The calculated oscillator strengths are direct from the quantum mechanics, eq. (1). The estimated oscillator strengths use the calculated oscillator strengths and the approximation of eq. (23).

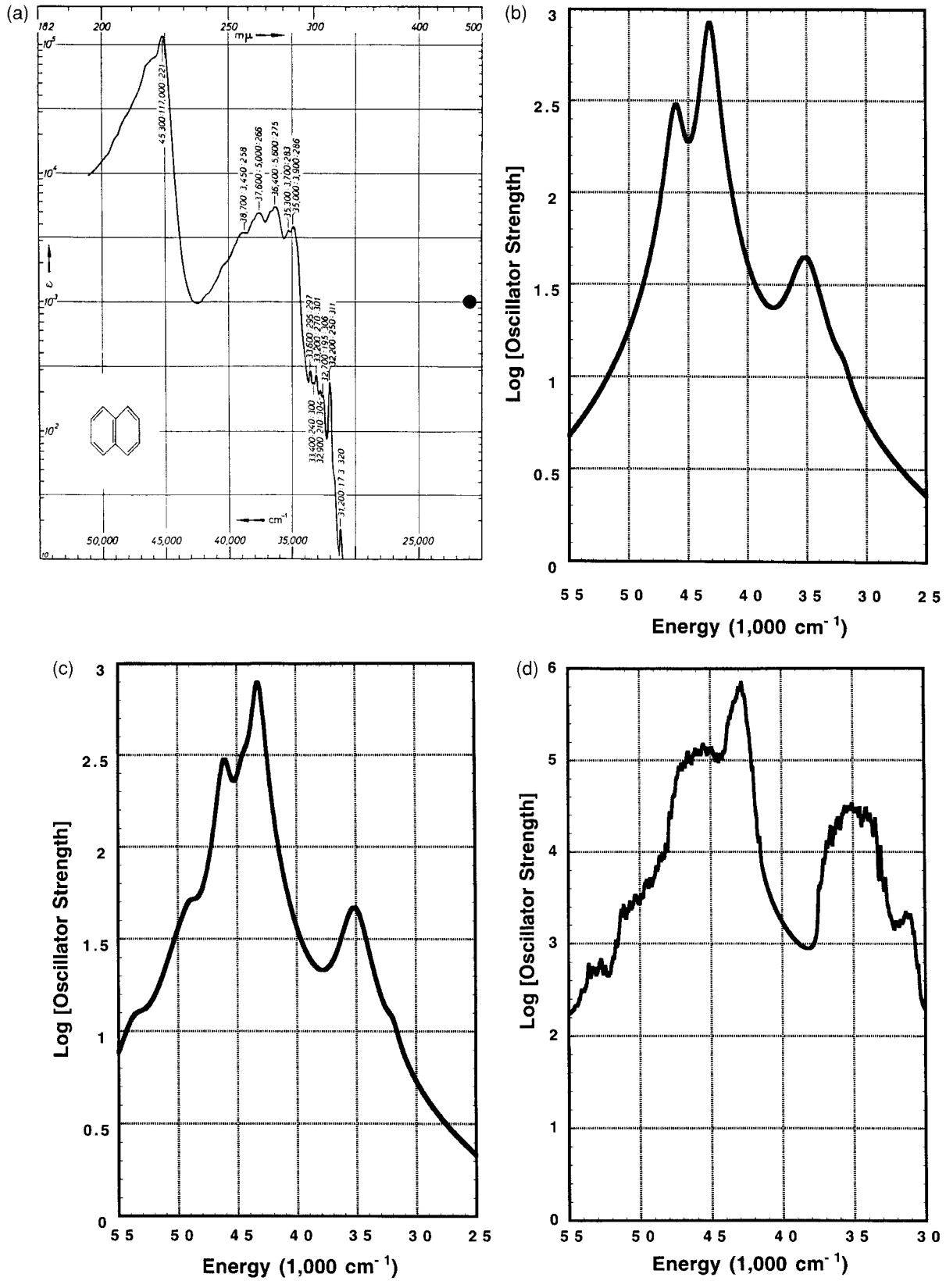


**FIGURE 5.** Naphthalene spectra. (A) Experimental spectra. (B) Bandwidth results. (C) Bandwidth including estimated vibronic borrowing results. (D) Molecular dynamics results.

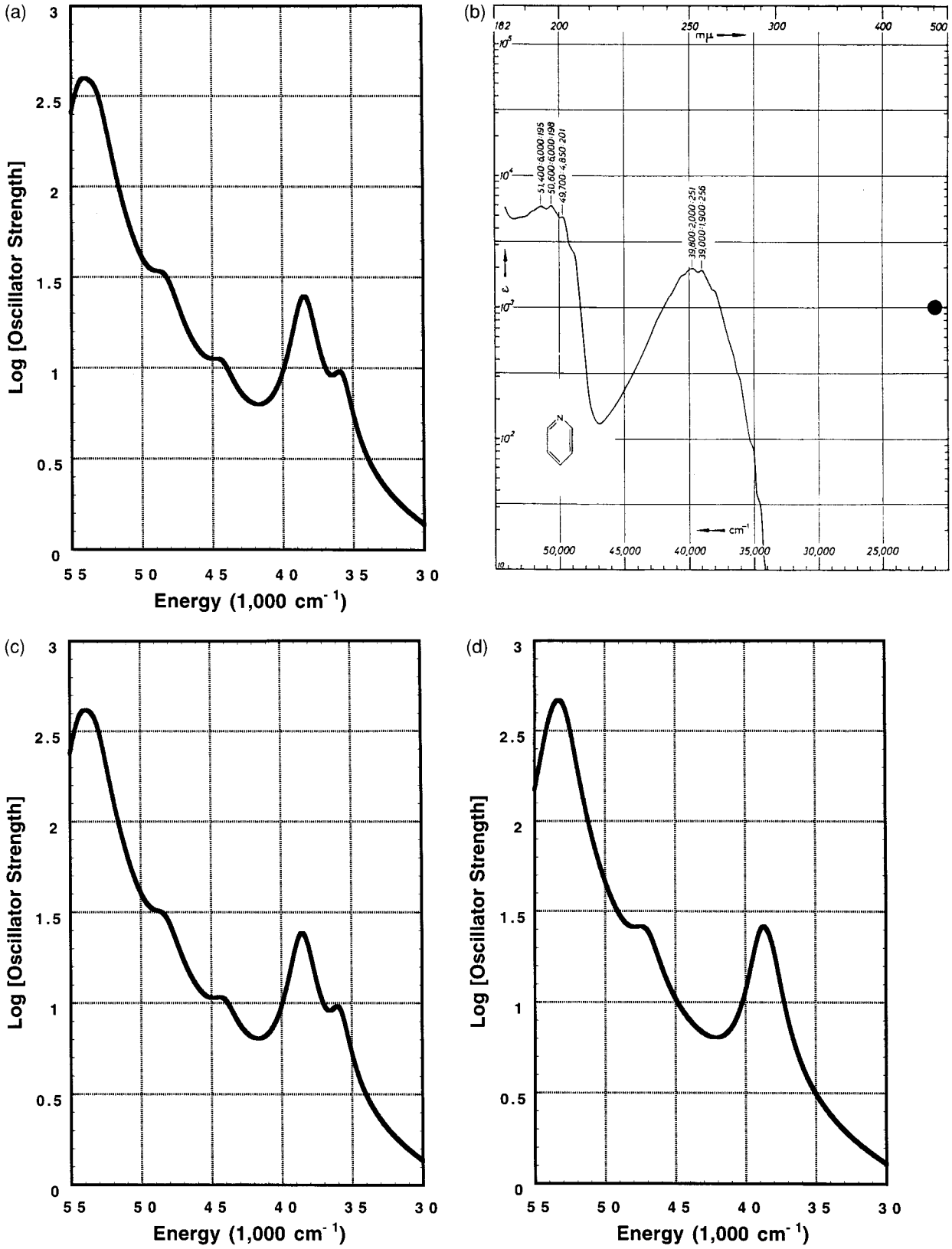


**FIGURE 6.** Pyridine spectra. (A) Gas phase results. (B) Experimental spectra: hexane. (C) Reaction field results: cyclohexane. (D) Reaction field results: water. (E) Experimental spectra: water. (F) Reaction field supermolecule results.

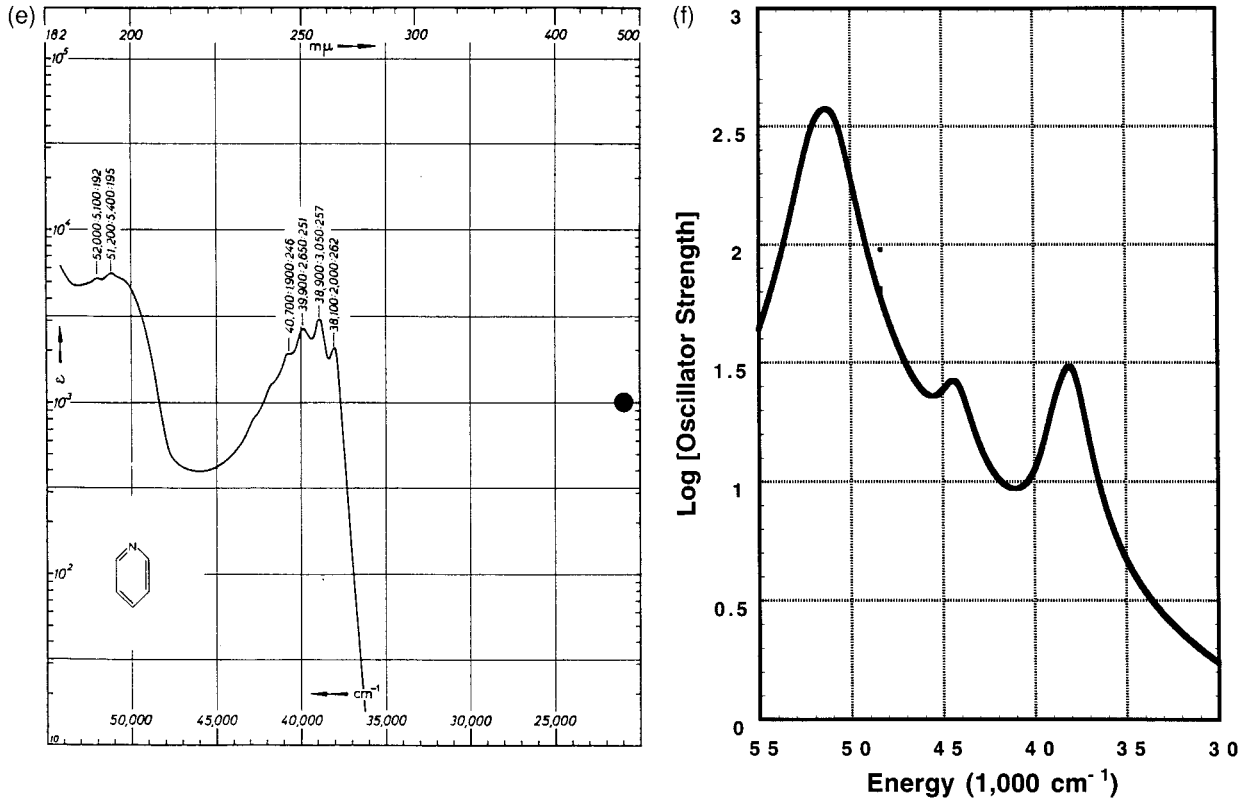


**FIGURE 6.** (Continued).

calculations that actually model explicitly bound water. This is a good indicator that a single $Z'$ parameter should be sufficient for modeling all solvents.

The spectrum of pyridazine is also well reproduced using the empirical bandwidth approximation (see Fig. 8 and Table VI).

While the spectra calculated for these three molecules correctly models changes to the band shape, the calculated changes are not as pronounced as they are in the experimental spectra. We are currently parameterizing $Z'$ to better reproduce these differences.

## Conclusion

A simple model for determining the bandwidth for molecular electronic spectroscopy has been developed and examined. The model has been shown

**TABLE IV.**
**Comparison of Different Solvents for Pyridine (All Numbers Listed in 1000 cm$^{-1}$).[a]**

| | | Gas phase | | Nonpolar | | Polar | | Polar + $H_2O$ | |
|---|---|---|---|---|---|---|---|---|---|
| | Exp. | Energy | Width | Energy | Width | Energy | Width | Energy | Width |
| $^1B_2$ | 34.7 | 35.8 | 1.6 | 35.9 | 1.6 | 38.1 | 1.5 | 36.9 | 1.6 |
| $^1B_1$ | 38.5 | 38.5 | 1.9 | 38.5 | 1.9 | 38.8 | 1.9 | 38.0 | 1.9 |
| $^1A_2$ | | 44.4 | 2.0 | 44.1 | 2.1 | 47.1 | 2.1 | 44.3 | 2.0 |
| $^1A_1$ | 49.7 | 48.4 | 2.3 | 48.3 | 2.3 | 47.8 | 2.3 | 48.4 | 2.5 |
| $^1A_1$ | 55.0 | 53.3 | 2.2 | 53.3 | 2.1 | 53.0 | 2.0 | 51.0 | 2.3 |
| $^1B_1$ | 56.4 | 54.4 | 2.0 | 54.3 | 2.0 | 53.7 | 2.0 | 51.9 | 2.3 |

[a] The symmetry labels were calculated from the $C_{2v}$ point group by ZINDO for all of the above calculations except for the reaction field + explicit water.

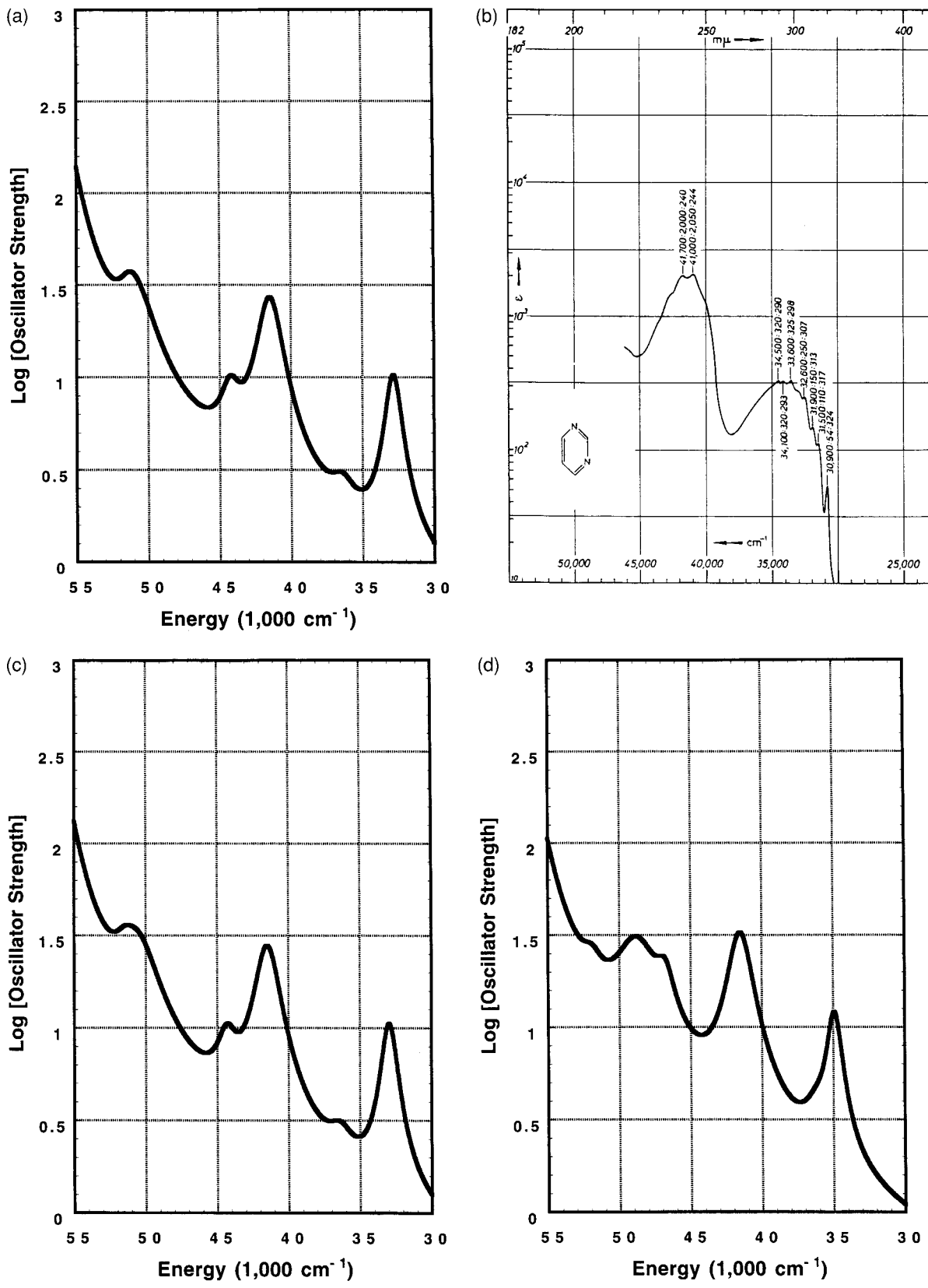


**FIGURE 7.** Pyrimidine spectra. (A) Gas phase results. (B) Experimental spectra: hexane. (C) Reaction field results: Cyclohexane. (D) Reaction field results: water. (E) Experimental spectra: water. (F) Reaction field supermolecule results.

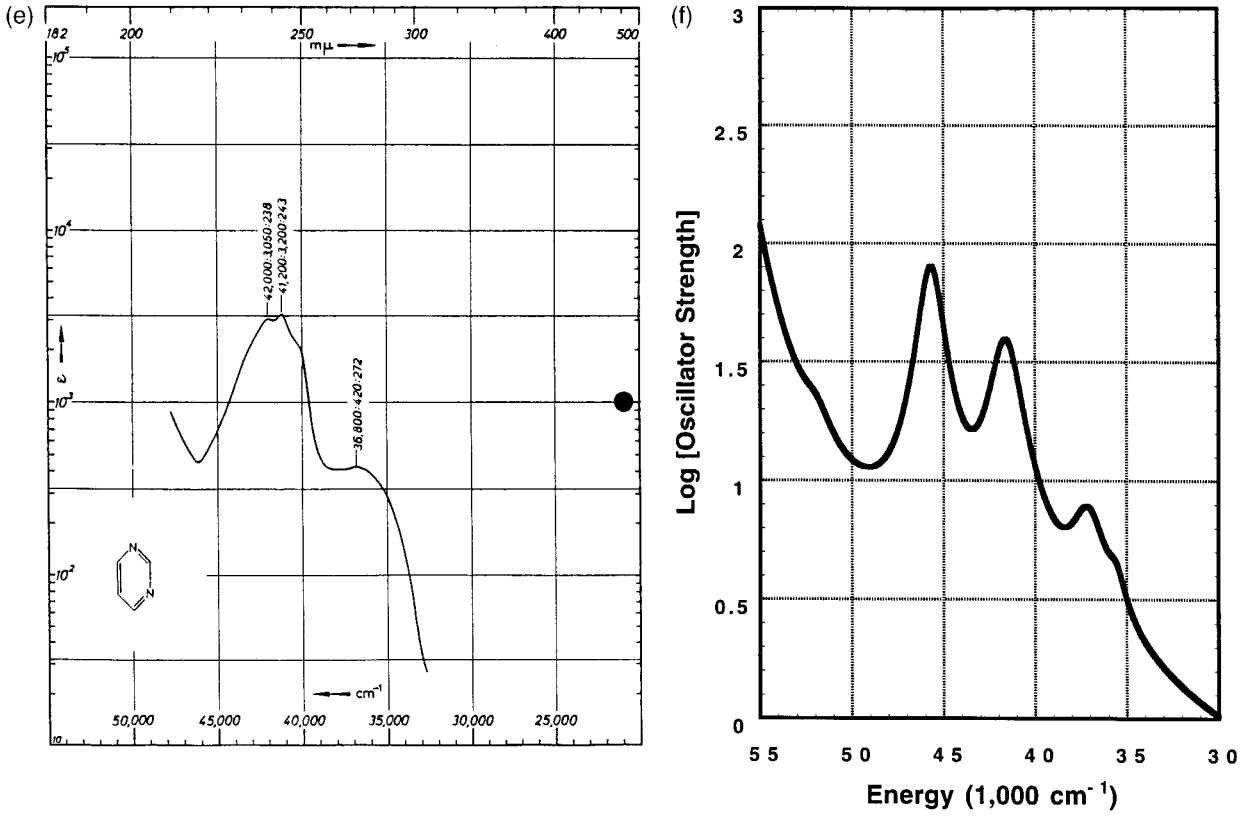


**FIGURE 7.** (Continued).

**TABLE V.**
**Comparison of Different Solvents for Pyrimidine (All Numbers Listed in 1000 $cm^{-1}$).[a]**

| | | Gas phase | | Nonpolar | | Polar | | Polar + $2H_2O$ | |
|---|---|---|---|---|---|---|---|---|---|
| | Exp. | Energy | Width | Energy | Width | Energy | Width | Energy | Width |
| $^1B_2$ | 31.0 | 32.9 | 1.2 | 33.0 | 1.2 | 34.9 | 1.1 | 35.6 | 1.1 |
| $^1A_2$ | | 36.4 | 1.8 | 36.4 | 1.9 | 36.2 | 2.0 | 37.1 | 2.0 |
| $^1B_1$ | 40.3 | 41.5 | 1.8 | 41.5 | 1.8 | 41.5 | 1.8 | 41.6 | 1.8 |
| $^1A_2$ | | 44.3 | 1.5 | 44.3 | 1.4 | 46.8 | 1.4 | 45.7 | 1.5 |
| $^1A_1$ | 51.1 | 50.9 | 2.8 | 50.6 | 2.9 | 48.8 | 3.4 | 49.1 | 3.5 |
| $^1B_2$ | 52.3 | 51.3 | 1.5 | 51.5 | 1.5 | 51.9 | 1.5 | 52.0 | 1.8 |
| $^1A_1$ | 56.2 | 56.2 | 2.0 | 56.3 | 2.0 | 56.7 | 1.9 | 56.2 | 2.0 |
| $^1B_1$ | 58.5 | 56.9 | 1.9 | 56.9 | 1.9 | 56.7 | 2.0 | 57.3 | 2.0 |

[a] The symmetry labels were calculated from the $C_{2v}$ point group by ZINDO for all of the above calculations except for the reaction field + explicit water.

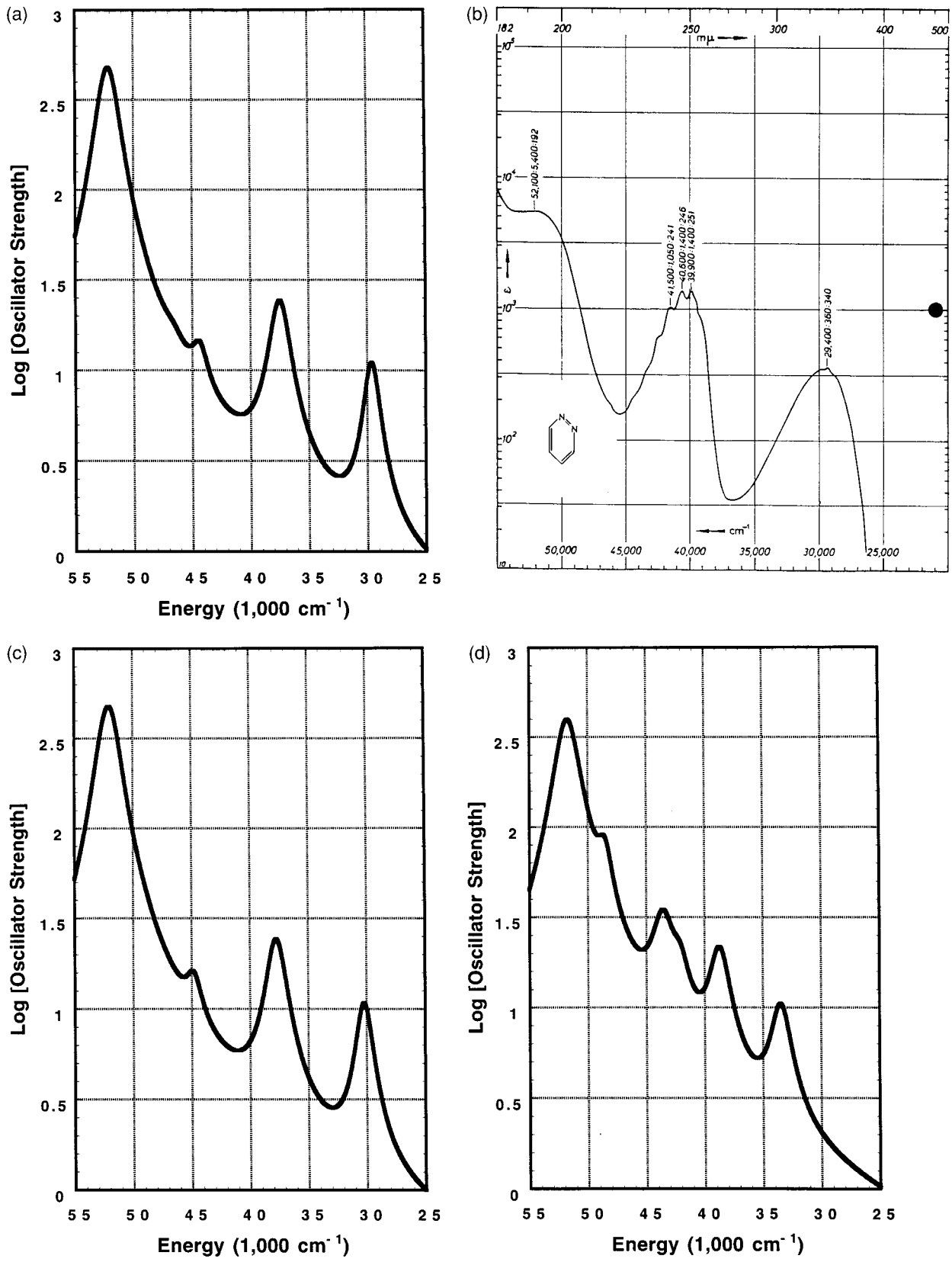


**FIGURE 8.** Pyridazine spectra. (A) Gas phase results. (B) Experimental spectra: hexane. (C) Reaction field results: cyclohexane. (D) Reaction field results: water. (E) Reaction field supermolecule results.

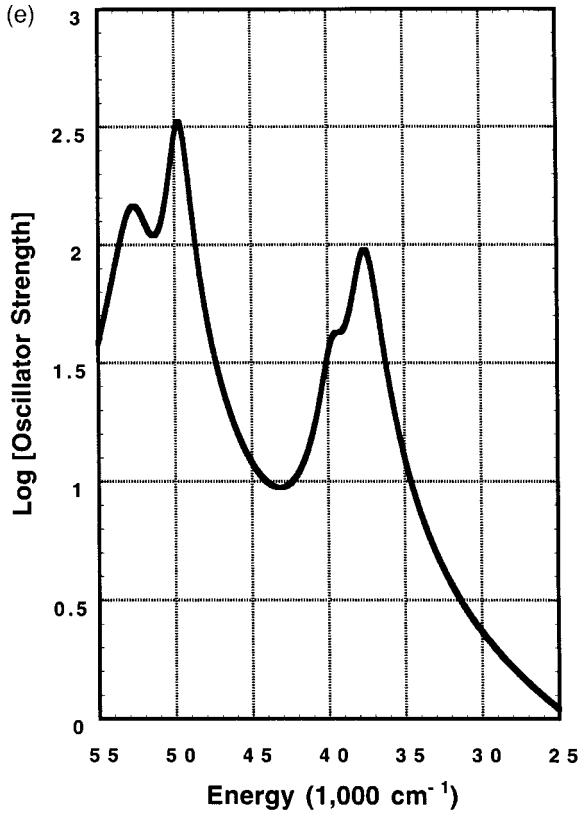


**FIGURE 8.** (Continued).

to reproduce the appearance of the experimental spectra for small organic molecules. Although this method does not reproduce the spectra as well as the stochastic method we describe, it does an adequate job and requires only fraction of the time. This model shows great promise for predicting the appearance of the spectra of large molecular systems in which stochastic calculations on such systems would simply be too expensive for the additional accuracy obtained.

This method has only two free parameters, which might be temperature and solvent dependent, although our preliminary studies suggest that this dependence is minor.

## References


1. R. G. Parr, *Quantum Theory of Molecular Electronic Structure*, Benjamin, Boston, 1963.
2. M. C. Zerner, *Problem Solving in Computational Molecular Sciences*, NATO ASI Series, Dordrecht.
3. (a) J. E. Ridley and M. C. Zerner, *Theor. Chim. Acta*, **32**, 111 (1973); (b) M. C. Zerner, G. H. Loew, R. F. Kirchner, and U. T. Mueller-Westerhoff, *J. Am. Chem. Soc.*, **102**, 589 (1980); (c) J. C. Culberson, P. Knappe, N. Rosch, and M. C. Zerner, *Theor. Chim. Acta*, **71**, 21 (1987); (d) J. D. Baker and M. C. Zerner, *Chem. Phys. Lett.*, **175**, 192 (1990).
4. (a) H. Nakatsuji, M. Komari, and O. Kitao, *Chem. Phys. Lett.*, **142**, 447 (1987); (b) H. Nakatsuji, O. Kitao, and T. Yonezawa, *J. Chem. Phys.*, **83**, 723 (1985); (c) H. Nakatsuji, J.-Y. Hasegawa, and M. Hada, *J. Chem. Phys.*, **104**, 2321 (1996).
5. (a) J. F. Stanton and R. J. Bartlett, *J. Chem. Phys.*, **97**, 7029 (1993); (b) for a review of couple-cluster methods, see R. J. Bartlett and J. F. Stanton, In *Reviews of Computational Chemistry*, *Vol. 5*, K. Lipkowitz and D. B. Boyd, Eds., VCH, New York.
6. (a) P. E. Siegbahn, A. Heiberg, B. O. Roos, and B. Levy, *Phys. Scr.*, **21**, 323 (1980); (b) B. O. Roos, P. R. Taylor, and P. E. Siegbahn, *Chem. Phys.*, **48**, 157 (1980).
7. J. Karwowski, *Int. J. Quantum Chem.*, **51**, 425 (1994).
8. (a) D. Bielinska-Waz and J. Karowski, *Phys. Rev. A*, **55**, 1067 (1995); (b) D. Bielinski-Waz and J. Karowski, *Advances in Quantum Chemistry*, Vol. 28, Academic Press, San Diego, CA, 1997.


**TABLE VI.**
**Comparison of Different Solvents for Pyridazine (All Numbers Listed in 1000 cm$^{-1}$).[a]**

| | | Gas phase | | Nonpolar | | Polar | | Polar + $2H_2O$ | |
|---|---|---|---|---|---|---|---|---|---|
| | Exp. | Energy | Width | Energy | Width | Energy | Width | Energy | Width |
| $^1B_1$ | 26.6 | 29.6 | 1.5 | 30.2 | 1.5 | 33.5 | 1.8 | 33.7 | 1.9 |
| $^1A_2$ | 39.5 | 37.4 | 1.6 | 37.9 | 1.6 | 42.1 | 1.6 | 37.6 | 1.7 |
| $^1A_1$ | | 37.5 | 1.9 | 37.7 | 1.9 | 38.7 | 1.9 | 39.7 | 1.9 |
| $^1A_2$ | | 44.4 | 1.5 | 44.8 | 1.5 | 48.6 | 1.4 | 43.3 | 1.5 |
| $^1B_2$ | | 46.6 | 2.0 | 46.3 | 2.0 | 43.5 | 2.0 | 49.7 | 1.9 |
| $^1B_2$ | ~ 50 | 52.1 | 2.0 | 51.9 | 2.0 | 51.8 | 2.0 | 50.2 | 1.9 |
| $^1B_1$ | | 52.1 | 1.7 | 52.4 | 1.7 | 57.3 | 1.8 | 52.8 | 3.1 |
| $^1A_1$ | | 52.4 | 2.0 | 52.3 | 2.0 | 51.8 | 2.6 | 54.3 | 3.3 |

[a] The symmetry labels were calculated from the $C_{2v}$ point group by ZINDO for all of the above calculations except for the reaction field + explicit water.

9. (a) P. J. Campagnola, D. J. Lavrich, M. J. DeLuca, and M. A. Johnson, *J. Chem. Phys.*, **94**, 5240 (1991); (b) A. Baczynski and D. Radomska, *J. Fluorescence*, **5**, 91 (1995).
10. (a) M. Klessinger and J. Michl, *Lichtabsorption and Photochemie Organischer Molekule*, VCH, New York, 1989; (b) D. A. McQuarrie, *Statistical Mechanics*, Harper Collins, New York, 1976.
11. (a) J. Blair, K. Krough-Jespersen, and R. Levy, *J. Am. Chem. Soc.*, **111**, 6948 (1989); (b) R. Levy, D. B. Kitchen, J. Blair, and K. Krough-Jespersen, *J. Phys. Chem.*, **94**, 4470 (1990); (c) J. Gao, *J. Am. Chem. Soc.*, **116**, 9324 (1994).
12. (a) K. Coutinho and S. Canuto, *Int. J. Quantum Chem.* (in press); (b) K. Coutinho, S. Canuto, and M. C. Zerner, *Int. J. Quantum Chem.* (in press).
13. (a) V. Luzhkov and A. Warshel, *J. Am. Chem. Soc.*, **112**, 4491 (1991); (b) A. Warshel, *J. Phys. Chem.*, **83**, 4912 (1979); (c) S. E. DeBolt and P. A. Kollman, *J. Am. Chem. Soc.*, **112**, 7515 (1990); (d) J. Zeng, N. S. Hush, and J. R. Reimer; *J. Phys. Chem.*, **100**, 9561 (1996).
14. H. Eyring, J. Walter, and G. E. Kimball, *Quantum Chemistry*, John Wiley & Sons, New York, 1944.
15. S. J. Weiner, P. A. Kollman, D. A. Case, U. C. Singh, C. Ghio, G. Alagona, S. Profeta, and P. Weiner, *J. Am. Chem. Soc.*, **106**, 765 (1984).
16. (a) K. B. Wiberg, *Terrahedron*, **24**, 1083 (1968); (b) M. C. Zerner and R. G. Parr, *J. Chem. Phys.*, **69**, 3858 (1978); (c) K. Jug, *J. Comput. Chem.*, **5**, 555 (1984).
17. J. B. Foresman, M. Head-Gordon, J. A. Pople, M. J. Fritsch, *J. Chem Phys.*, **96**, 135 (1992).
18. *UV Atlas of Organic Compounds*, (Organischer Verbindungen), Plenum Press, New York, 1966.
19. A. Broo, G. Pearl, and M. C. Zerner, *J. Phys. Chem.*, **101**, 2478 (1997).
20. ZINDO, A semiempirical quantum chemistry program by M. C. Zerner and coworkers, University of Florida, Gainesville, FL, distributed by MSI Technologies, San Diego, CA, www.msi.com.
21. N. Mataga and K. Nishimoto, *Z. Chem. Phys.*, **13**, 140 (1957).
22. (a) M. M. Karelson and M. C. Zerner, *J. Chem. Phys*, **96**, 6949 (1992); (b) N. Rösch and M. C. Zerner, *J. Phys. Chem.*, **98**, 5817 (1994); (c) M. M. Karelson and M. C. Zerner, *J. Am. Chem. Soc.*, **112**, 9405 (1990).